Supporting information

High-Rate and Long-Life Flexible Aqueous Rechargeable Zinc-Ion Battery Enabled by Hierarchical Core-Shell Heterostructures

Ziming Xu[a], Wenyuan Zhang[a,b], Xianzhen Wang[a], Yuxin Li[a], Jinwen Fu[a], Yongbao Feng[a], Wenbin Gong[b], Jiabin Guo[c,d], Pan Xue[e], Qiulong Li[a*]

a. College of Materials Science and Engineering, Nanjing Tech University, Nanjing 211816, China

b. School of Physics and Energy, Xuzhou University of Technology, Xuzhou 221018, China

c. Key Laboratory of Multifunctional Nanomaterials and Smart Systems, Advanced Materials Division, Suzhou Institute of Nano-Tech and Nano-Bionics, Chinese Academy of Sciences, Suzhou, 215123, China

d. School of Electronic Science & Engineering, Southeast University, Nanjing, 210096, China

e. School of Chemistry and Chemical Engineering, Yangzhou University, Yangzhou, 225002, China

Corresponding Author: qlli@njtech.edu.cn (Q. Li)

Material and methods

Material

Titanium tetrachloride (TiCl$_4$, 99%), manganese sulfate monohydrate (MnSO$_4$·H$_2$O, 99%), sodium sulfate anhydrous (Na$_2$SO$_4$, 99%) were purchased from Shanghai Aladdin Biochemical Technology Co., Ltd. Boric acid (H$_3$BO$_3$, 99.8%), sodium acetate (C$_2$H$_3$NaO$_2$, 99%) were obtained from Sinopharm Chemical Reagent, China. Hydrochloric acid (HCl, 36-38%), zinc sulfate heptahydrate (ZnSO$_4$·7H$_2$O, 99.5%) were purchased from Yonghua chemical Co., Ltd. The carbon cloth (CC-W0S1009) was purchased from Sinero. Absolute ethanol alcohol (CH$_3$CH$_2$OH) was from Wuxi Yasheng Chemical Company. Deionized water (H$_2$O) was RO grade water made by BioSafer pure water machine in the laboratory. Each of these chemicals was used directly without any further purification.

Preparation of Zn NSs/CC anode

Zn NSs/CC were prepared by electrochemical deposition with a three-electrode system. The CC was acted as working electrode, Pt sheet as counter electrode and Ag/AgCl as reference electrode. In 50 mL of aqueous solution including 6.25 g ZnSO$_4$·7H$_2$O, 6.25 g Na$_2$SO$_4$ and 1 g H$_3$BO$_3$. The electrochemical deposition current density and time were -40 mA cm^{-2} and 600 s, respectively.

Preparation of CMC-ZnSO$_4$ electrolyte

The ZnSO$_4$-CMC gel electrolyte was synthesized by dissolving 10 g ZnSO$_4$·7H$_2$O, 0.5 g MnSO$_4$·H$_2$O and 3 g CMC in 80 mL deionized water and stirring vigorously at 85 °C for 90 min.

Characterization

The morphologies of the as-fabricated samples were observed by scanning electron microscopy (SEM; Hitachi S-4800, 5 kV). The microstructures of the as-prepared samples were characterized by transmission electron microscopy (TEM; FEI Tecnai G2 F20 S-Twin) operating at an acceleration

voltage of 200 kV. Raman spectra are collected using a Raman spectrometer (horiba evolution) to monitor molecular states and structures. The chemical compositions and phase structures of the as-prepared samples were analyzed on an ESCALAB MKII X-ray photoelectron spectrometer (XPS) using non-monochromatized Mg Kα X-rays as the excitation source and a Rigaku D/MAX2500 V system using Cu Kα radiation ($\lambda = 1.5418$ Å) to obtain the X-ray diffraction (XRD) patterns.

Electrochemical measurements

The electrochemical evaluation was carried out by assembling into a CR2032-type coin cell, using the TiN@MnO$_2$ NWAs/CC wafer as a cathode, waterman GF/D glass fiber as a separator, Zn foil as anode and 2 M ZnSO$_4$·7H$_2$O with 0.2 M MnSO$_4$·H$_2$O solution as the electrolyte. The CV and EIS were tested using an electrochemical workstation (CHI 760E). The GCD performance and GITT measurements are obtained through a battery testing system (Land 2001A) with a voltage ranging from 0.8 V to 1.8 V at 28 °C. Other comparative samples used the same method to assemble batteries to test electrochemical performance. The capacity (C), energy density (E), and power density (P) were calculated according to the following equations:

$$C_A = \frac{I\Delta t}{3600A} \tag{1}$$

$$E_A = C_A \times V_P \tag{2}$$

$$P_A = 3600 \times \frac{E_A}{\Delta t} \tag{3}$$

Where A is the mass of active material in aqueous ZIBs. I, Δt and V$_p$ represent the discharge current, discharge time, and voltage platform, respectively.

The ion diffusion coefficient (D) was studied according to the relationship between Z' and $\omega^{-1/2}$ via the following equation:

$$D = \frac{R^2 T^2}{2A^2 n^4 F^4 C^2 \sigma^2}$$

(4)

where R, T, A, n, F and C represent gas constant (8.314 J mol^{-1}·K^{-1}), testing temperature (298 K), electrode area, reactive electron number per chemical formula, Faraday's constant (96500 C mol^{-1}), and the molar concentration of ions, respectively. Warburg factor (σ) was equaled to the slopes of Z'-$\omega^{-1/2}$, and the Z' is imaginary resistance, and ω is the angular speed.
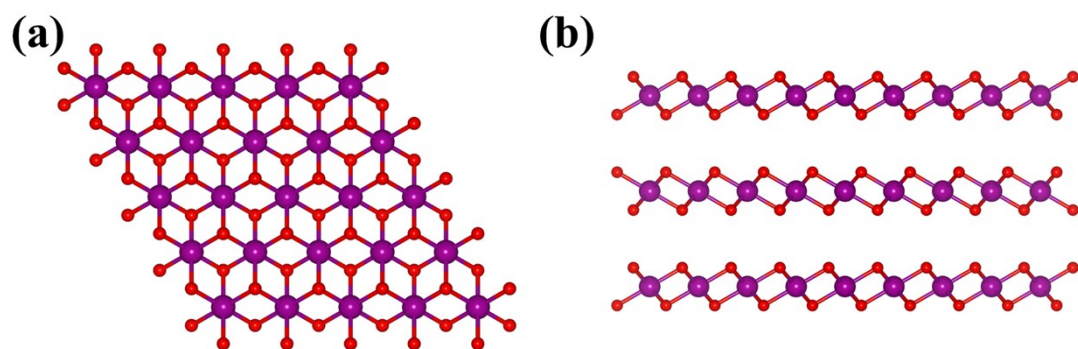
Figure S1 Crystal structure of MnO_2 from side view (a) and top view (b).
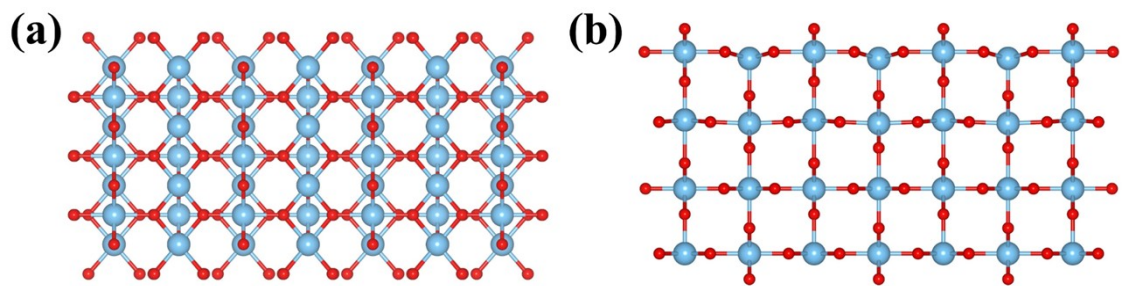
Figure S2 Crystal structure of TiO_2 from side view (a) and top view (b).
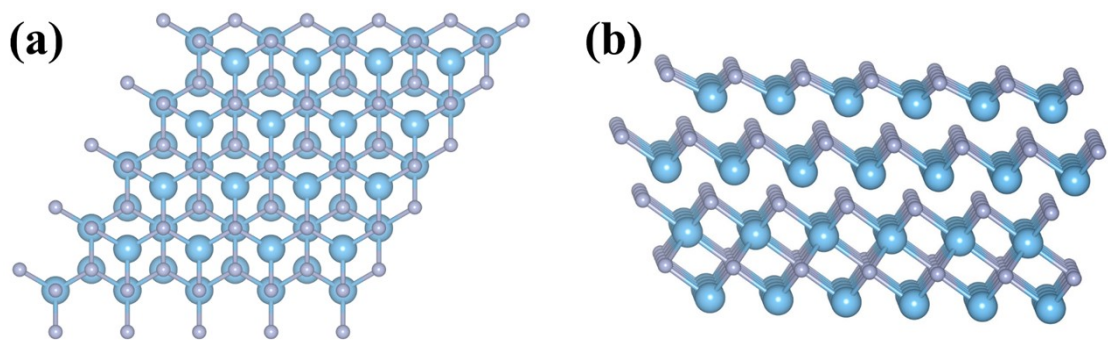
Figure S3 Crystal structure of TiN from side view (a) and top view (b).
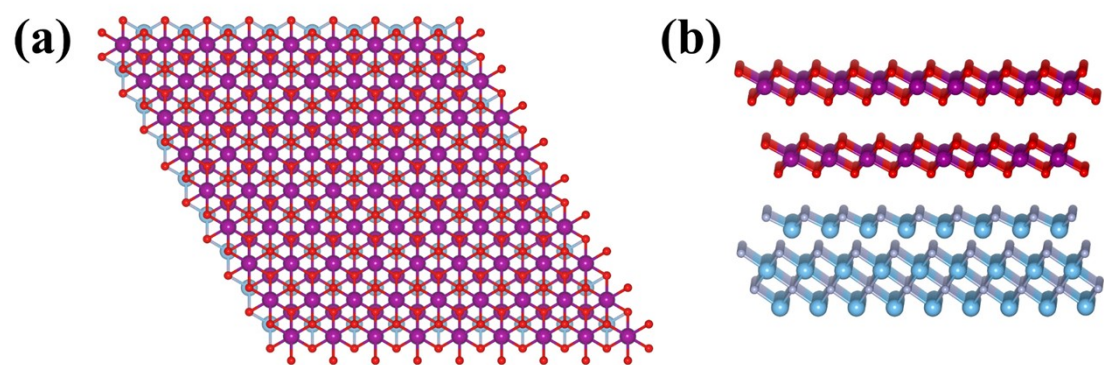
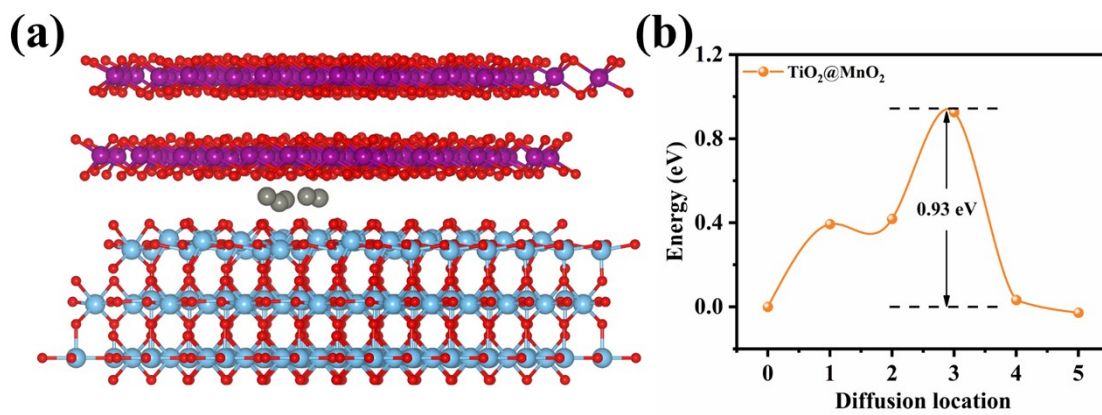**Figure S4** Crystal structure of TiN@MnO$_2$ from side view (a) and top view (b).

Figure S5 Schematic diagram of TiO$_2$@MnO$_2$ for diffusion path of Zn^{2+} (a) and diffusion barrier (b).
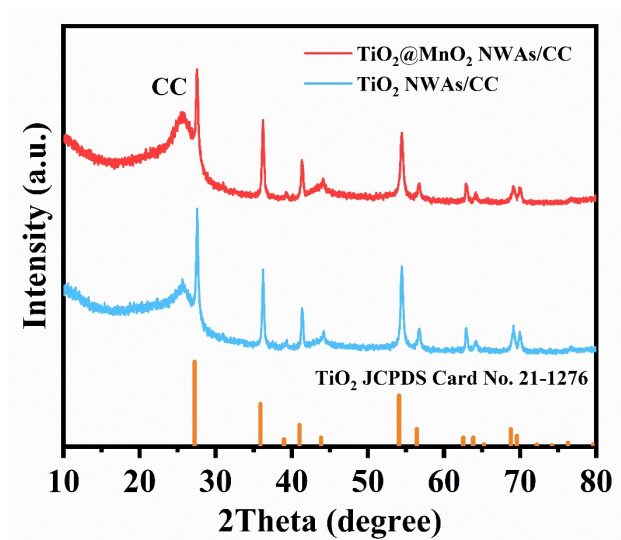
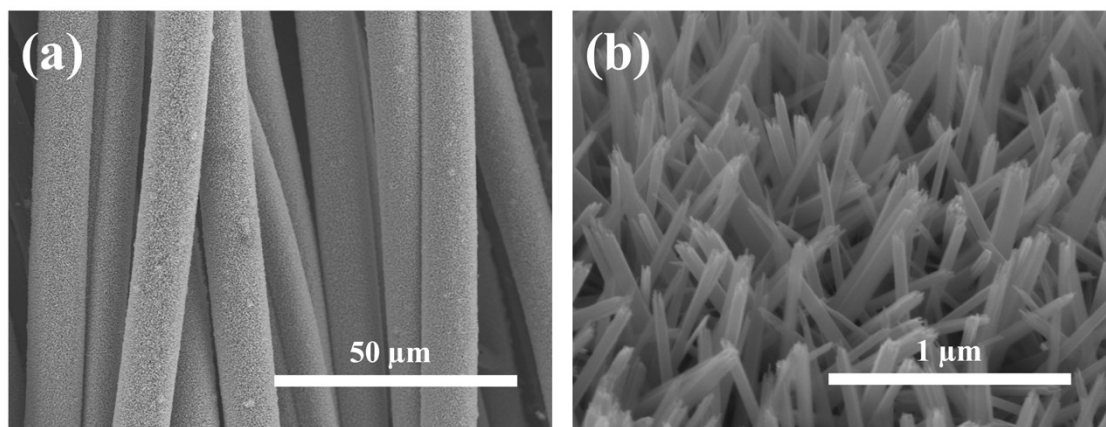**Figure S6** XRD patterns of TiO$_2$@MnO$_2$ NWAs/CC and TiO$_2$ NWAs/CC.

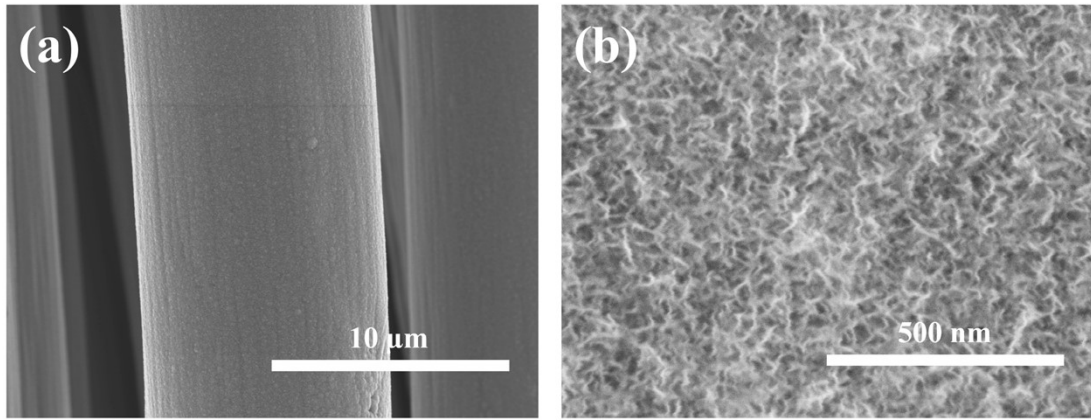**Figure S7** (a, b) SEM images of TiO_2 NWAs/CC at different magnifications.

Figure S8 (a, b) SEM images of MnO$_2$ NSs/CC at different magnifications.
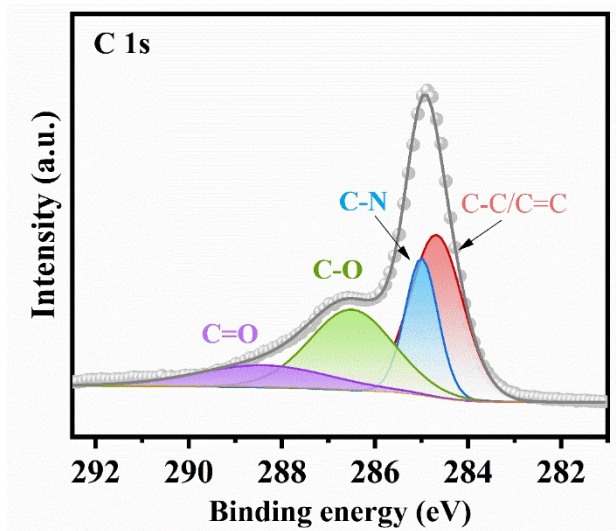
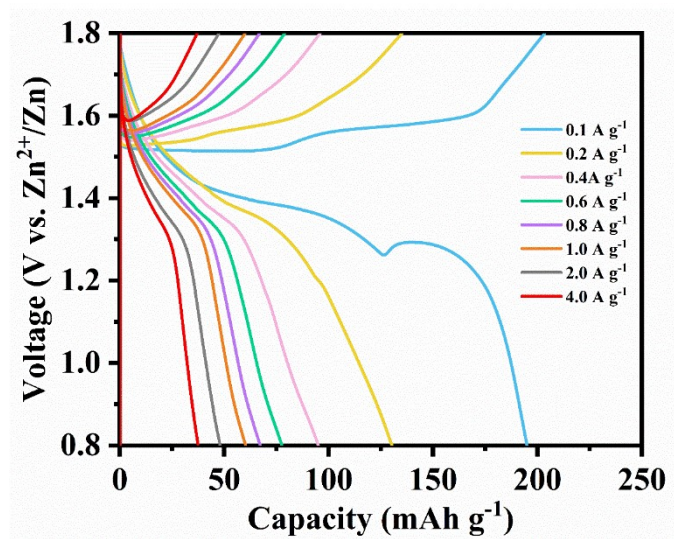**Figure S9** High-resolution C 1s XPS spectrum of TiN@MnO$_2$ NWAs/CC.

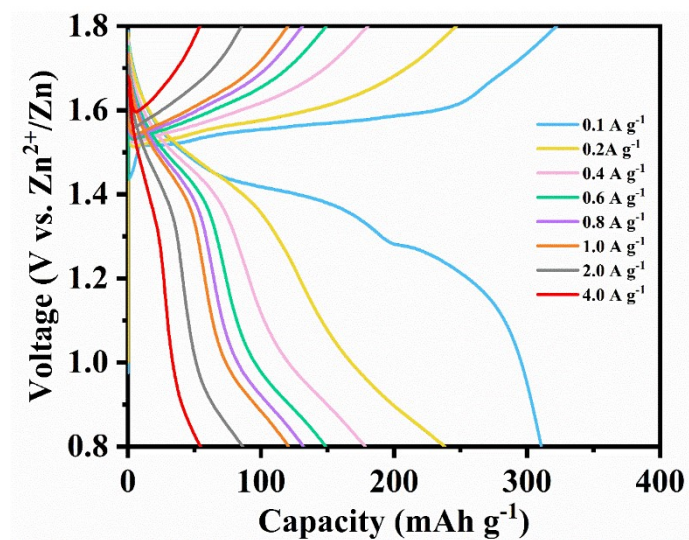**Figure S10** GCD curves of the MnO$_2$ NSs/CC electrode at different current densities.

Figure S11 GCD curves of the $TiO_2@MnO_2$ NWAs/CC electrode at different current densities.
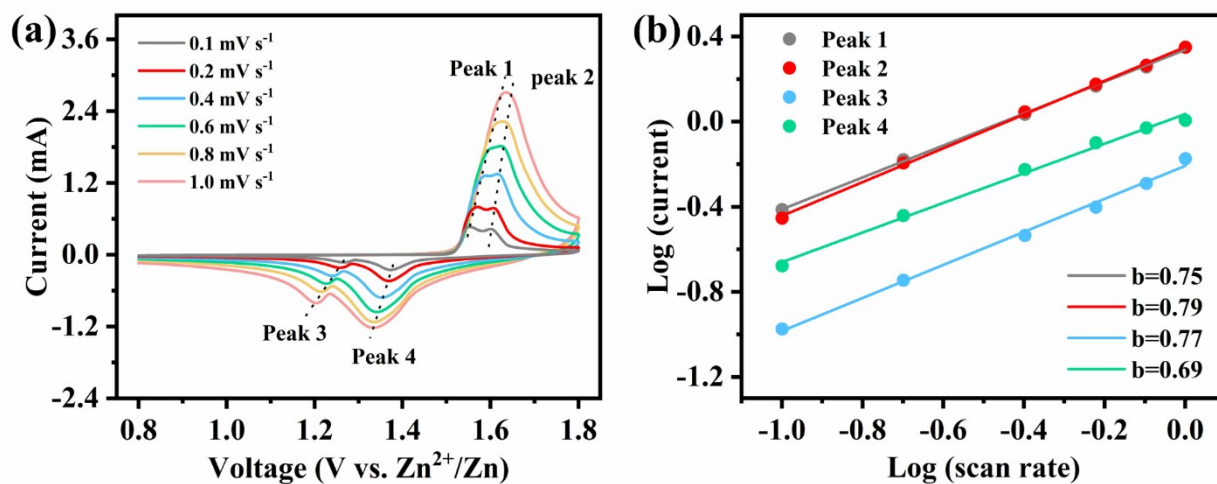
Figure S12 The electrochemical kinetics of MnO$_2$ NSs/CC batteries during the charge/discharge process. (a) CV curves at different scan rate. (b) The relationship between log(i) and log(v) during the scan rate is 0.1-1 mV s^{-1}.
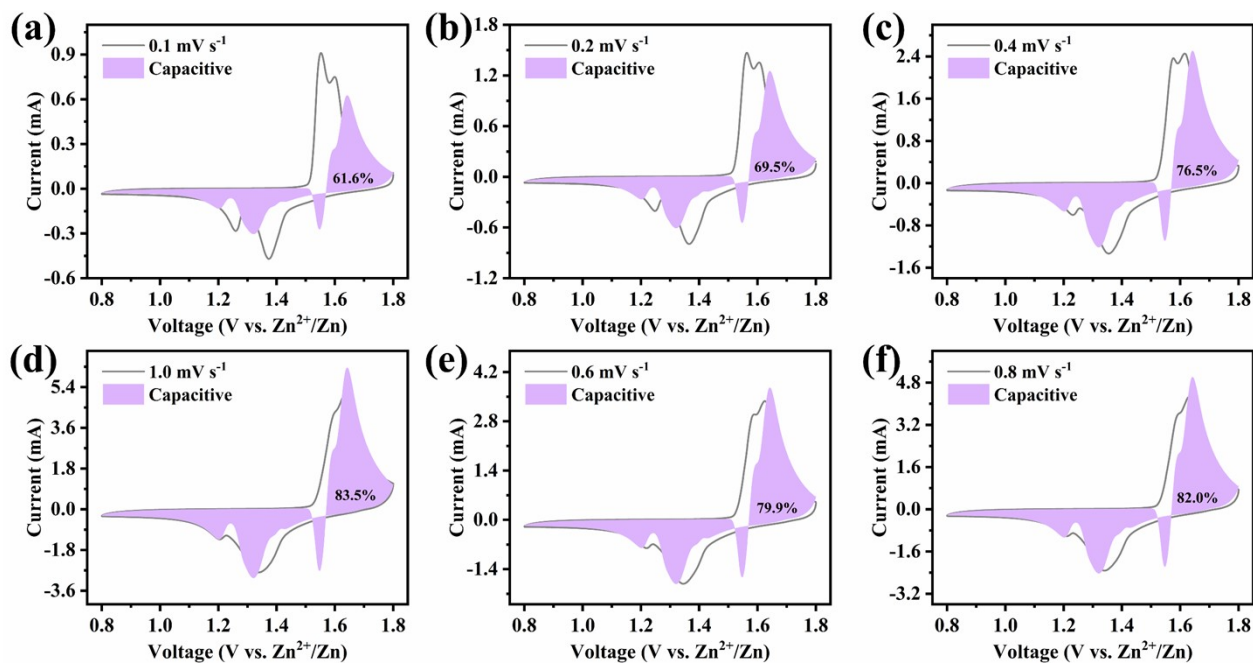
Figure S13 The capacitance contribution of TiN@MnO$_2$ NWAs/CC at different scan rates of 0.1 mV s^{-1} (a), 0.2 mV s^{-1} (b), 0.4 mV s^{-1} (c), 0.6 mV s^{-1} (d), 0.8 mV s^{-1} (e) and 1.0 mV s^{-1} (f).
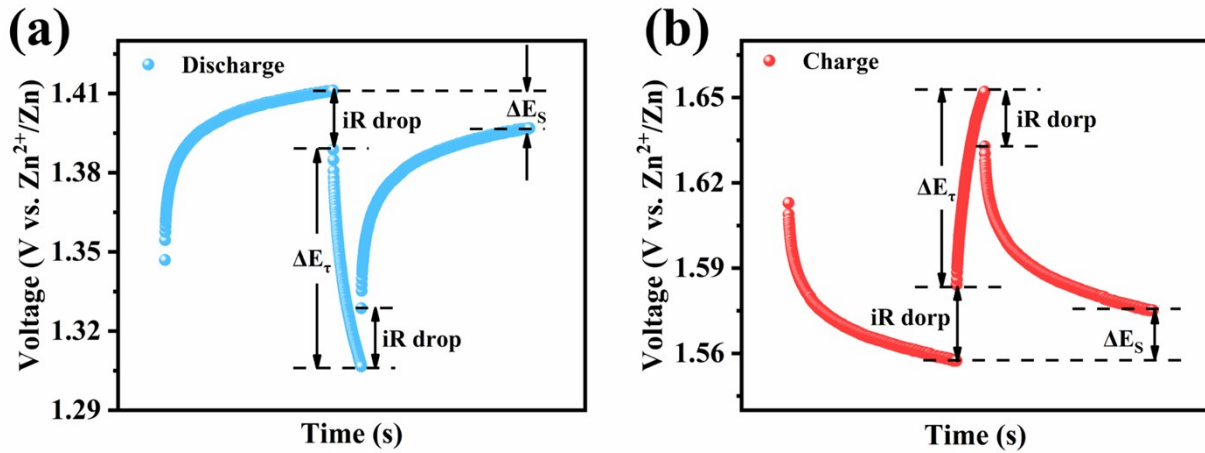
Figure S14 Schematic illustration for a single step in GITT measurement: discharge (a) and charge (b).

GITT is used to calculate the ion diffusion coefficient (D), and D is calculated based on the following equation:[1, 2]

$$D = \frac{4}{\pi\tau}\left(\frac{m_B V_M}{M_B S}\right)^2\left(\frac{\Delta E_S}{\Delta E_\tau}\right)^2$$

$$= \frac{4}{\pi\tau}\left(\frac{m_B V}{n M_B S}\right)^2\left(\frac{\Delta E_S}{\Delta E_\tau}\right)^2$$

$$= \frac{4}{\pi\tau}\left(\frac{m_B}{\rho S}\right)^2\left(\frac{\Delta E_S}{\Delta E_\tau}\right)^2$$

where m_B, V_M and M_B are the mass (g), molar volume (cm^3 mol^{-1}) and molar mass (g mol^{-1}) of the electrode, respectively. τ is the duration current pulse time (s), S is the contact area (cm^2) between electrode and electrolyte, ρ is the density of the active material (g cm^{-3}), ΔE_S is the voltage change between two adjacent equilibrium states, and ΔE_τ is the voltage change due to galvanostatic charging/discharging. A current density of 0.1 A g^{-1} is applied to the electrode with τ = 5 min and then stood for 30 min without current impulse.
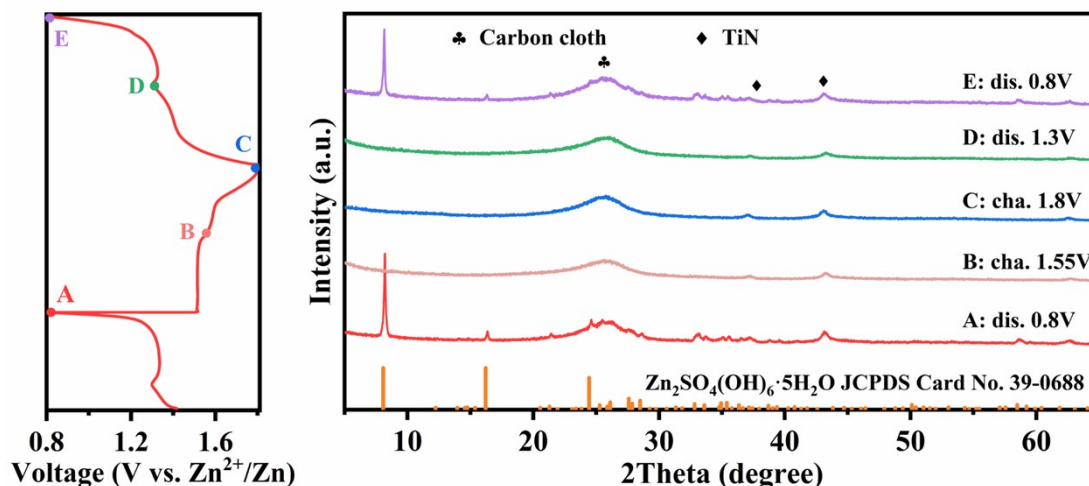
Figure S15 The GCD curves of the first and second cycles and the corresponding ex situ XRD patterns.

Figure S15 depicts the GCD curves of the first and second cycles, as well as their corresponding ex-situ XRD patterns. Following discharge to 0.8 V, an obvious $Zn_4SO_4(OH)_6 \cdot 5H_2O$ (JCPDS Card No. 39-0688) phase appears, implying the insertion of H^+ into the electrodes. This observation is consistent with previous reports for many Mn-based materials.[3, 4] During the subsequent charge and discharge process, the diffraction peak of $Zn_4SO_4(OH)_6 \cdot 5H_2O$ disappears after charging to 1.8 V (point C) and reappears after full discharge (point E), demonstrating that $TiN@MnO_2$ NWAs/CC has good reversibility during charging and discharging processes.
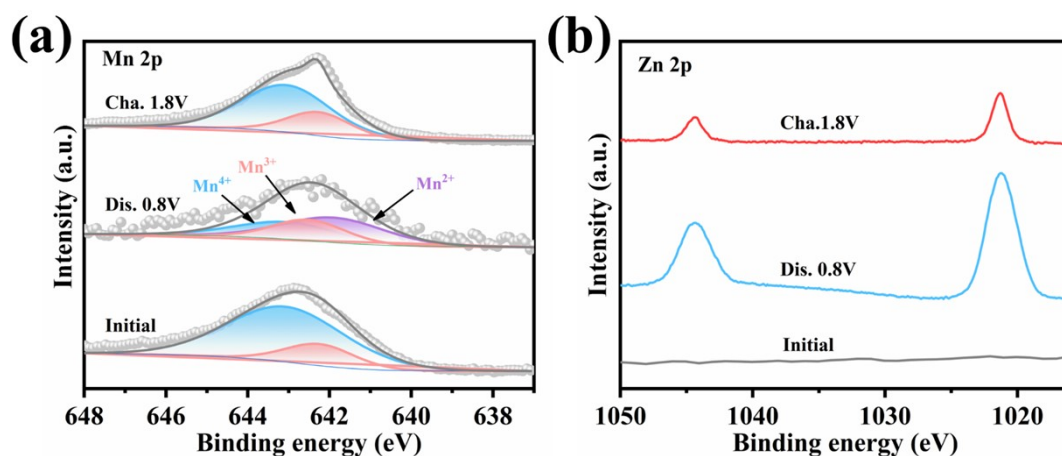
Figure S16 High-resolution XPS spectra of Mn 2p (a) and Zn 2p (b) at different states.

The Mn valence state and Zn content in TiN@MnO$_2$ NWAs/CC were revealed by ex-situ XPS analysis, as shown in Figure S16. A peak of Mn^{2+} appears upon discharge to 0.8 V, indicating that Mn is partially reduced. When charged to 1.8 V, Mn^{2+} is oxidized to Mn^{3+} and Mn^{4+}. In the Zn 2p XPS spectrum, no zinc is found in the initial state. But when fully discharged to 0.8 V, a strong signal about Zn appears, indicating that Zn^{2+} is intercalated into the electrode. When charged to 1.8 V, the signal strength of zinc is significantly reduced and the residual Zn signal may be due to adsorption of Zn^{2+} on the surface.
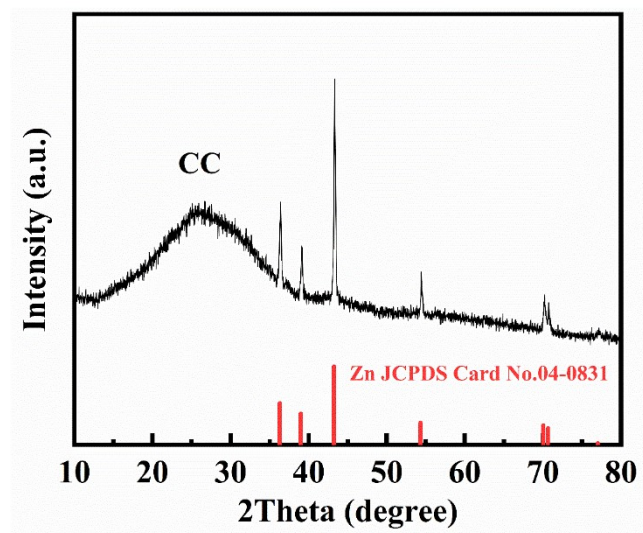
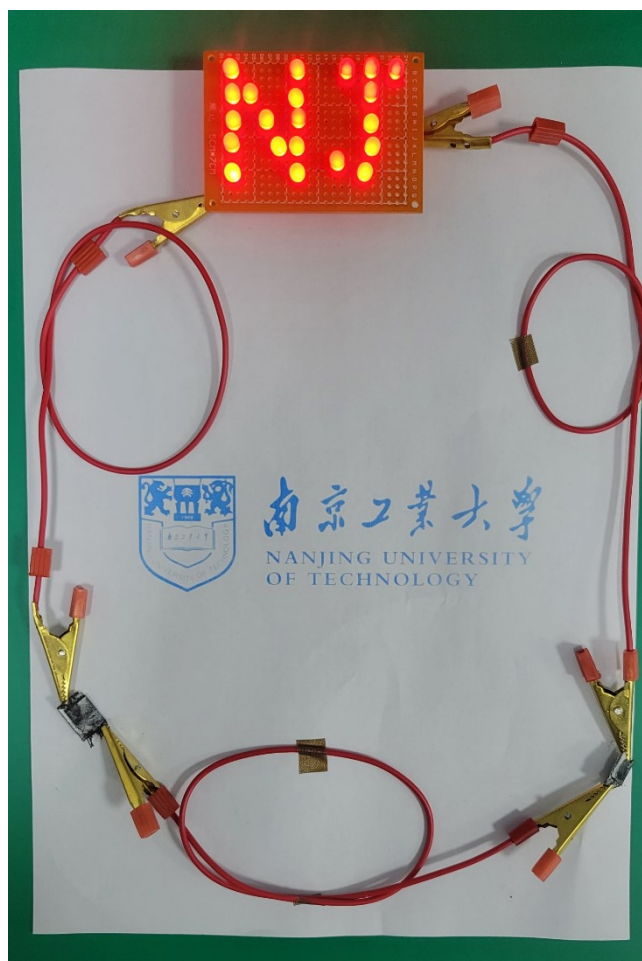**Figure S17** XRD pattern of Zn NSs/CC.

Figure S18 Photo image of our as-assembled all-solid-state ZIBs lighting parallel LEDs.

References:

1 Q. Tan, X. Li, B. Zhang, X. Chen, Y. Tian, H. Wan, L. Zhang, L. Miao, C. Wang, Y. Gan, J. Jiang, Y. Wang, and H. Wang, *Adv. Energy. Mater*., 2020, **10**, 2001050.

2 Y. Zhao, P. Zhang, J. Liang, X. Xia, L. Ren, L. Song, W. Liu, X. Sun, *Energy Storage Mater.*, 2022, **47**, 424-433.

3 D. Zhang, J. Cao, X. Zhang, N. Insin, S. Wang, J. Han, Y. Zhao, J. Qin and Y. Huang, *Adv. Funct. Mater.*, 2021, **31**, 2009412.

4 G. Fang, C. Zhu, M. Chen, J. Zhou, B. Tang, X. Cao, X. Zheng, A. Pan and S. Liang, *Adv. Funct. Mater.*, 2019, **29**, 1808375.